J Biomol NMR (2013) 56:77–84
DOI 10.1007/s10858-013-9735-9

COMMUNICATION

Parallel acquisition of 3D-HA(CA)NH and 3D-HACACO spectra

Jithender G. Reddy · Ramakrishna V. Hosur

Received: 24 February 2013 / Accepted: 25 April 2013 / Published online: 5 May 2013

Abstract We present here an NMR pulse sequence with 5 independent incrementable time delays within the frame of a 3-dimensional experiment, by incorporating polarization sharing and dual receiver concepts. This has been applied to directly record 3D-HA(CA)NH and 3D-HACACO spectra of proteins simultaneously using parallel detection of ^{1}H and ^{13}C nuclei. While both the experiments display intra-residue backbone correlations, the 3D-HA(CA)NH provides also sequential '$i - 1 \rightarrow i$' correlation along the ^{1}Hα dimension. Both the spectra contain special peak patterns at glycine locations which serve as check points during the sequential assignment process. The 3D-HACACO spectrum contains, in addition, information on prolines and side chains of residues having H–C–CO network (i.e., ^{1}Hβ, ^{13}Cβ and ^{13}COγ of Asp and Asn, and ^{1}Hγ, ^{13}Cγ and ^{13}COδ of Glu and Gln), which are generally absent in most conventional proton detected experiments.

Keywords Multi-dimensional NMR · Dual receivers · Parallel acquisition · Different indirect dimension chemical shift encoding · Proteins · Complete ^{1}H ^{13}C and ^{15}N backbone resonance assignment

Electronic supplementary material The online version of this article (doi:10.1007/s10858-013-9735-9) contains supplementary material, which is available to authorized users.

J. G. Reddy · R. V. Hosur (✉)
Department of Chemical Sciences, Tata Institute of Fundamental Research, Homi Bhabha Road, Mumbai 400005, India
e-mail: hosur@tifr.res.in
URL: http://www.tifr.res.in/~hosur/

R. V. Hosur
UM-DAE Centre for Excellence in Basic Sciences, Mumbai University Campus, Kalina, Santa Cruz, Mumbai 400098, India

Nuclear magnetic resonance (NMR) spectroscopy has proven ability to provide in-depth information on structure, dynamics, and interactions of proteins, which is so crucial to understand biological functions at atomic mechanistic details, by virtue of the fact that it provides many reporters of information in terms of various nuclei along the protein chain. This has led to the development of a plethora of multidimensional NMR experiments which establish correlations among the various nuclei (Kanelis et al. 2001; Permi and Annila 2004; Wagner 1997). While higher dimensionality enhances information content by enabling monitoring of larger number of nuclei, for example, 7-dimensional automated projection spectroscopy (7D-APSY) (Hiller et al. 2007) in one experiment, it also increases data acquisition time and requires complicated data analysis. The best and most commonly used strategy has been to record multiple three dimensional experiments with different information contents (Kanelis et al. 2001). The challenge today, in the context of emerging fields of 'targeted proteomics' (Marx 2013), 'targeted metabolomics' and 'drug discovery programs', is to extract maximum multidimensional spectral information, as rapidly as possible to keep pace with the data coming out from genome sequencing consortia. This has led to many new ideas for rapid data acquisition, such as reduced dimensionality approaches (Szyperski et al. 1993; Reddy and Hosur 2012), single scan methods (Frydman et al. 2002), different sampling approaches (Atreya and Szyperski 2005), sensitivity enhancement approaches (Schanda et al. 2006; Pervushin et al. 2002), automation of data analysis (Lescop and Brutscher 2009; Borkar et al. 2011), etc. to name a few. The most recent development in this context is the use of multiple receivers for acquiring data simultaneously on more than one nucleus, for example, ^{1}H and ^{13}C, in the same experiment (Kupce et al. 2006; Kupce 2011). With

these, the magnetization transfer pathway can be split into different paths that can be manipulated separately and recorded. The different data sets can be recorded either in parallel or in sequential fashion and the sequential acquisition method has been explored rather more extensively (Kupce et al. 2010; Kupce and Freeman 2008, 2011; Chakraborty et al. 2012). However, one drawback of sequential acquisition is that the length of one of the direct detection periods would be restricted, and this would limit the resolution along that dimension. On the other hand, in parallel acquisition, signals from both the pathways are detected simultaneously at the end of the pulse sequence (Kupce and Kay 2012), and this does not have any length limitation. The distinctive feature of the experiment presented here, compared to the previously reported dual receiver experiments (Kupce and Kay 2012) is the introduction of different chemical shifts during the second indirect dimension evolution. As a result, a total of five different nuclei are encoded in the entire pulse sequence. In other words a five dimensional spectral information covering almost all the nuclei along the protein backbone can be recorded in the time of one three dimensional experiment. This enables rapid and unambiguous complete assignment of the protein backbone, on one hand, and would facilitate extensive interaction studies with different molecules within a practical time frame, on the other.

The general approach in our scheme is shown in Fig. 1. A Pulse sequence would start with creating transverse magnetization on one nucleus (preparation period) which further undergoes evolution for the time period 't_1' (first indirect dimension). The magnetization present on the frequency labeled nucleus undergoes polarization sharing between two directly bonded nuclei. This creates two different magnetization flow pathways which can be manipulated separately for two different mixing periods (mixing 1 and mixing 1′) and chemical shift encoding during the second indirect dimension evolution (during t_2 and t_2' periods). The magnetization is then relayed to correspondingly bonded nuclei for detection (shown as t_3 and t_3' periods). Thus there are five independent incrementable time periods, which could encode different chemical shifts. The entire data from the two pathways are recorded as two different 3D-data sets and Fourier transformed separately to produce two 3D-spectra, which together encode 5 chemical shifts.

Figure 2a presents a pulse sequence incorporating the above ideas for resonance assignment in proteins. The magnetization transfer pathway resulting in two 3D-spectra is summarized in Fig. 2b. The experiment starts with creating Hα transverse magnetization followed by INEPT (Morris and Freeman 1979) polarization transfer to directly bonded Cα carbon (at the end of A + B + C in Fig. 2a). During this INEPT step the α-proton is frequency-labeled

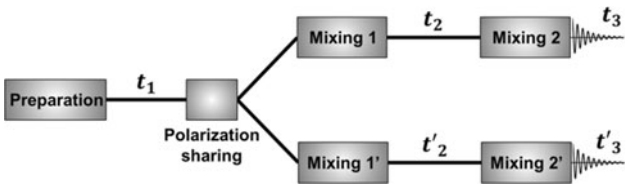

Fig. 1 Schematic approach for designing NMR pulse sequence with 5 independent incrementable time delays within the frame of a 3-dimensional experiment, by incorporating polarization sharing and dual receiver concepts

('t_1' period embedded in semiconstant-time manner) (Grzesiek and Bax 1993). Between the gradients G1 and G2, the Cα magnetization which is anti-phase with respect to Hα converts into in-phase magnetization by Hα–Cα J-coupling evolution for 'κ' time period. This Cα transverse magnetization now evolves under the influence of one-bond Cα–CO coupling for '$2\tau_C$' time period and under the influence of one-bond and two-bond N–Cα couplings for '$2\tau_{CN}$' time period, simultaneously. This is the crucial step where polarization sharing happens between two different nuclei. After the 90° pulse on Cα, followed by crusher gradient G2 the magnetization terms relevant for final detection are:

$$\begin{aligned}&\left\{-2\cos\left[2\pi\left({}^1J_{C\alpha CO}\right)\tau_C\right]\left\{\cos\left[2\pi\left({}^2J_{NC\alpha}\right)\tau_{CN}\right]\right.\right.\\&\times\sin\left[2\pi\left({}^1J_{NC\alpha}\right)\tau_{CN}\right]\left(C\alpha_Z^i\right)\left(N_Z^i\right)+\cos\left[2\pi\left({}^1J_{NC\alpha}\right)\tau_{CN}\right.\\&\left.\left.\times\sin\left[2\pi\left({}^2J_{NC\alpha}\right)\tau_{CN}\right]\left(C\alpha_Z^i\right)\left(N_Z^{i+1}\right)\right\}+2\sin\left[2\pi\left({}^1J_{C\alpha CO}\right)\tau_C\right]\right.\\&\times\cos\left[2\pi\left({}^1J_{NC\alpha}\right)\tau_{CN}\right]\times\cos\left[2\pi\left({}^2J_{NC\alpha}\right)\tau_{CN}\right]\left(C\alpha_Z^i\right)\left(CO_Z^i\right)\Big\}\\&\times\cos\left[2\pi\left({}^1J_{C\beta}\right)\tau_{CN}\right]\times\cos[(\Omega_{H\alpha})t_1]\times K_{Ca}\end{aligned}\qquad(1)$$

where, $K_{C\alpha}$ is a relaxation term (details are given in supplementary material). The two terms in Eq. (1), represented by operator terms $C\alpha_zN_z$ and $C\alpha_zCO_z$ evolve through the rest of the pulse sequence separately to generate the two pathways. Between gradient G2 and G3, $C\alpha_zN_z(i, i+1)$ terms evolve into in-phase $N_z(i, i+1)$ and also undergo chemical shift evolution for 't_2^N' in a constant time manner during '$2T_N$' time period (D + E + F in Fig. 2a). This magnetization is stored as in-phase $N_z(i, i+1)$ terms till gradient G5, after which it is transferred back to ^{1}HN for detection. This magnetization transfer pathway generates the 3D-HA(CA)NH data set with ^{1}Hα, ^{15}N and ^{1}HN chemical shifts.

The other term in Eq. (1), namely, $2C\alpha_zCO_z$ is manipulated by the scheme between gradients G3 and G5. It is converted to transverse anti-phase term '$2C\alpha_yCO_z$' which is then frequency labeled by Cα chemical shift evolution for 't_2^C' time period and then transferred to carbonyl carbon

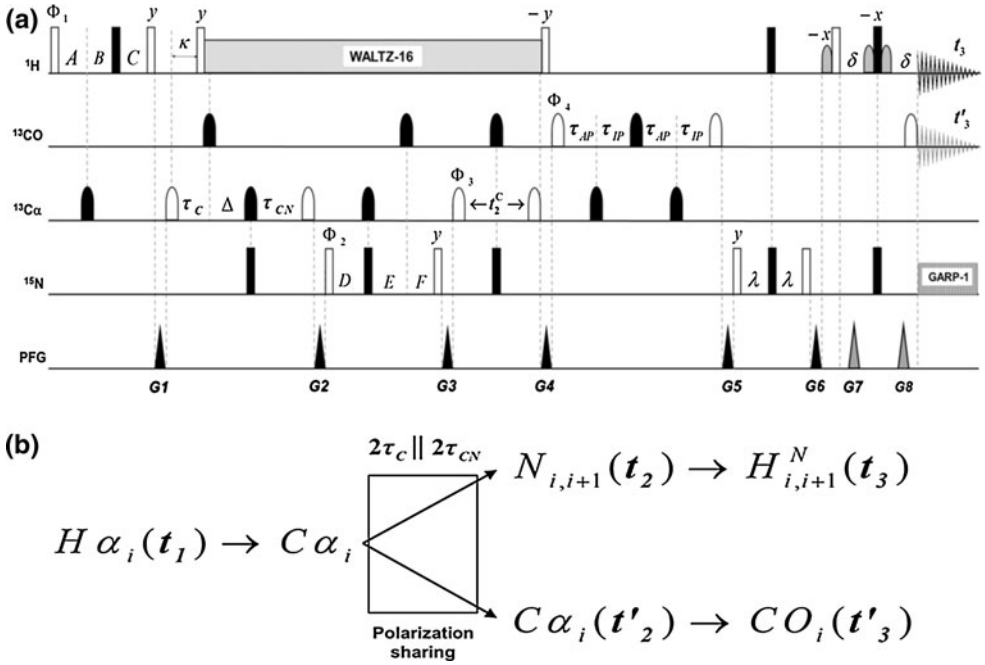

Fig. 2 **a** The pulse sequence for dual receiver 3D-HA(CA)NH‖3D-HACACO experiment, with parallel acquisition of ^{1}HN and ^{13}CO nuclei. *Hollow and filled* (*black*) *rectangular bars* represent non-selective 90° and 180° pulse, respectively. Unless indicated, the pulses are applied with phase 'x'. WALTZ-16 decoupling sequence (Shaka et al. 1983a, b) with field strength of 6.3 kHz is applied for proton decoupling, and ^{15}N decoupling using the GARP-1 sequence (Shaka et al. 1985) with the field strength 0.9 kHz is applied during acquisition. The pulse durations of the ^{13}Cα pulses (standard Gaussian cascade Q3 (180°) and Q5 (90°) pulses) (Emsley and Bodenhausen 1990) is adjusted so that they cause minimal perturbations of carbonyl carbons. The 180° ^{13}CO shaped pulse had a standard Gaussian cascade Q3 pulse profile with minimal excitation of ^{13}Cα. The offset of ^{13}C carrier is kept at 54 ppm for effective excitation of the α-carbons. After gradient pulse G4, the offset is switched to 176 ppm (^{13}CO offset) for effective excitation of carbonyls and also for detection of ^{13}CO at the end of the pulse sequence. The delays were set to A = 1.8 ms, B = 3 μs, C = 2.0 ms, κ = 2.2 ms, τ_{CN} = 12.5 ms, T_N = 14 ms, λ = δ = 2.7 ms, and Δ = τ_{CN} − τ_C. 'τ_C' period is optimized to 3.5 ms as discussed in the text. Chemical shift evolution in ^{1}Hα is achieved in a semi-constant manner (Morris and Freeman 1979) by varying A, B and C as: ΔA = t_1/2; ΔB = (t_1/2) − C/*ni* and ΔC = − C/*ni*, where *ni* = no. of complex points in 't_1'. The values for the individual periods containing 't_2' for 3D-HA(CA)NH were: D = T_N − (t_2^N/2), E = T_N, and F = t_2^N/2. The phase cycling for the experiment is Φ_1 = x, −x; Φ_2 = Φ_3 = 2(x), 2(−x) and Φ_{rec} = x, 2(−x), x (same for both ^{1}HN and ^{13}CO detection). In this experiment frequency discrimination in t_1 and t_2^N/t_2^C has been achieved using States-TPPI phase cycling (Marion et al. 1989) of Φ_1 and Φ_2/Φ_3, respectively, along with the receiver phase. The IPAP scheme (Ottiger et al. 1998; Permi and Annila 2004) is implemented for recording 3D-HACACO data set by setting $\Phi_4 = y$, $\tau_{IP} = \zeta$ = 4.5 ms and τ_{AP} = 0 ms to record the in-phase component and $\Phi_4 = -x$, $\tau_{IP} = \zeta/2$ and $\tau_{AP} = \zeta/2$ to record the anti-phase component. This has no effect on the ^{1}HN detected signal. The gradient (sine-bell shaped; 1 ms) levels are as follows: G1 = 50 %, G2 = G3 = G4 = 30 %, G5 = G6 = 80 % and G7 = G8 = 60 % of the maximum strength 53 G/cm in the z-direction. The recovery time after each gradient pulse was 160 μs. Before detection, WATERGATE sequence (Piotto et al. 1992) has been employed for better water suppression. **b** Practical approach for acquiring five dimensional information covering almost all the nuclei along the protein backbone in the time of one three dimensional experiment

by pair of 90° pulses on both Cα and CO. Then, in the following IPAP scheme (Ottiger et al. 1998; Andersson et al. 1998) this anti-phase $2C\alpha_zCO_y$ term, generates in-phase term, $2C\alpha_zCO_y \rightarrow CO_z$ for $\Phi_4 = y$, $\tau_{IP} = \zeta$, $\tau_{AP} = 0$ and anti-phase term, $2C\alpha_zCO_y \rightarrow 2C\alpha_zCO_z$ for Φ_4 = -*x*, $\tau_{IP} = \zeta/2$, $\tau_{AP} = \zeta/2$ where, $\zeta = [4(^{1}J_{C\alpha\text{-}CO})]^{-1}$ = 4.5 ms. Addition/subtraction of these two components results in observable ^{13}CO magnetization following the final carbonyl 90° pulse prior to detection. This pathway is responsible for a '^{13}Cα decoupled, ^{13}CO detected' 3D-HACACO spectrum with ^{1}Hα, ^{13}Cα, and ^{13}CO chemical shifts. In the experiment described here, we utilized ^{1}HN and ^{13}CO nuclei for parallel acquisition of two multi-dimensional data sets. The two-bond scalar coupling between ^{1}HN and ^{13}CO nuclei is small (Yang et al. 1999) (4.4 ± 0.4 Hz), and therefore decoupling of these nuclei from each other is not essential during parallel acquisition. The complete magnetization transfer on amino acid sequence and resulting 3D-HA(CA)NH and 3D-HACACO data sets are schematically shown in Fig. 3.

The special feature of the present experiment is that not only are the directly detected nuclei different, but also the indirectly detected nuclei in the second indirect dimension. In 3D-HA(CA)NH data set ^{15}N is labeled during t_2^N period, whereas, in 3D-HACACO data set ^{13}Cα is labeled during t_2^C period. Accordingly, there are two separate spectral

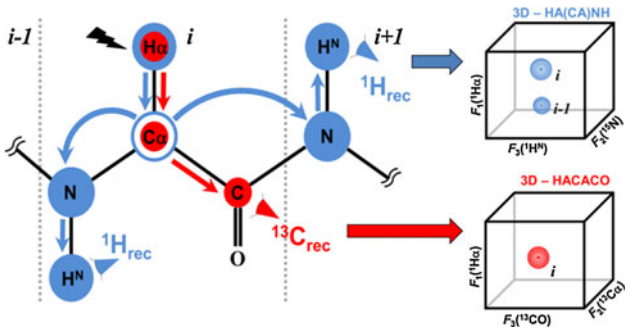

Fig. 3 Schematic representation of the complete magnetization transfer pathway and frequency labeling shown on amino acid sequence and resulting 3D-HA(CA)NH and 3D-HACACO spectra

widths and two separate time increments in the second indirect dimensions which of course, occur at different time points along the pulse sequence. The two indirect dimension time increments are related as ratio of their spectral widths in Hz:

$$\Delta t_2^C = (SW_N/SW_C) * \Delta t_2^N \quad (2)$$

the number of increments along the 't_2' dimension of both the data sets is the same.

The sensitivity of the experiments depends critically on the gyromagnetic ratio (γ) of the detected nucleus, which increases as $\gamma^{3/2}$. Therefore in theory, sensitivity of proton detected experiments is eight fold higher than that in carbon-detected experiments. In the present case, the two pathways for both of which the polarization comes from proton have different transfer efficiencies at the intervening steps, as also relaxation characteristics along the pathways. Thus, the resultant polarization arising due to sharing between the two pathways is not the same at the beginning of the two detection periods. Further, the sensitivity along carbon detection is reduced by a factor of 8. Therefore, in order to get similar intensities in the two spectra, which is necessary for optimizing signal averaging for meaningful benefits in both the spectra, polarization sharing will have to be adjusted so that a greater fraction goes into the carbon detection pathway than in the proton detection pathway (e.g. if initial proton polarization is 1.0 and is shared such that the polarizations just before detection are 0.11 and 0.88 along the ^{1}H and ^{13}C detection pathways, respectively, then the detected signals along the two pathways will be similar). The transfer efficiency functions and the parameters for optimization of 'τ_C' and 'τ_{CN}' time delays to obtain maximum intensities in both the 3D-data sets are discussed in detail in the supplementary material and resultant plots are shown in Fig. 4. The relative intensities in 3D-HA(CA)NH and 3D-HACACO spectra can be controlled by the optimization of 'τ_C' since the sensitivities of these data sets are proportional to $\cos(2\pi^1 J_{C\alpha CO}\tau_C)$and $\sin(2\pi^1 J_{C\alpha CO}\tau_C)$, respectively. One can optimize the 'τ_C' value to adjust the polarization sharing suitably. The sensitivity parameters [Eqs. (6) and (7) in supplementary material] as function of 'τ_C' period are shown in Fig. 4a. Considering the relaxation effects on the signal intensities and noting that transverse relaxation of Cα is very efficient, the optimization of the 'τ_{CN}' period, during which magnetization resides on Cα is also essential for obtaining good intensities. Figure 4b shows sensitivity parameters as a function of 'τ_{CN}' period. The vertical lines (gray color) in Fig. 4a, b indicate the optimal values for 'τ_C' and 'τ_{CN}' periods, respectively, for the present experiment.

At this stage it is worthwhile comparing the sensitivity of the experiment presented here (signal/noise ratios in the two 3D-spectra) vis-à-vis the sensitivities that would have been obtained had the two 3D-spectra been collected independently. For this purpose we have made a calculation of the transfer efficiencies in the two cases and plotted them also in Fig. 4. It appears that the sensitivity of the experiment presented here (solid lines in Fig. 4) would be

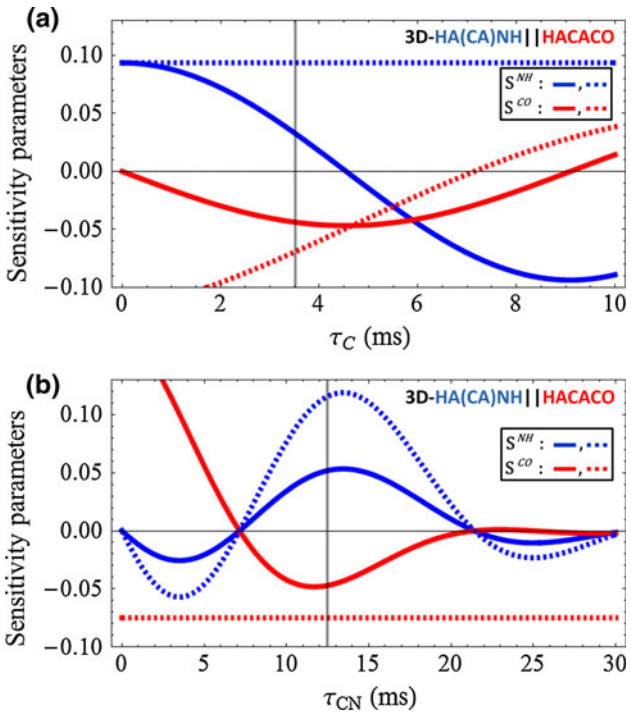

Fig. 4 Plots of sensitivity parameter functions S^{NH} and S^{CO} (discussed in the supplementary material) as a function of variables, 'τ_C' (**a**) and 'τ_{CN}' (**b**). Plots for experiment presented here and the individual experiments are shown in *solid* and *dotted lines*, respectively. The plots were calculated by using $^1J_{C\alpha-C\beta}$, $^1J_{C\alpha-CO}$, $^1J_{C\alpha-N}$, and $^2J_{C\alpha-N}$ values of 35, 55, 11, and 7 Hz, respectively. The values of transverse relaxation terms$R_2^{C\alpha}$, R_2^N and R_2^{CO} used here are 30, 15 and 10 s^{-1}, respectively. In **a**, the value of 'τ_{CN}' is 12. 5 ms, and in **b**, the value of 'τ_C' is 3.5 ms. *Vertical line* (*Gray*) shows the optimal value of 'τ_C' in (**a**) and of 'τ_{CN}' in (**b**) for obtaining maximum intensity in both the spectra

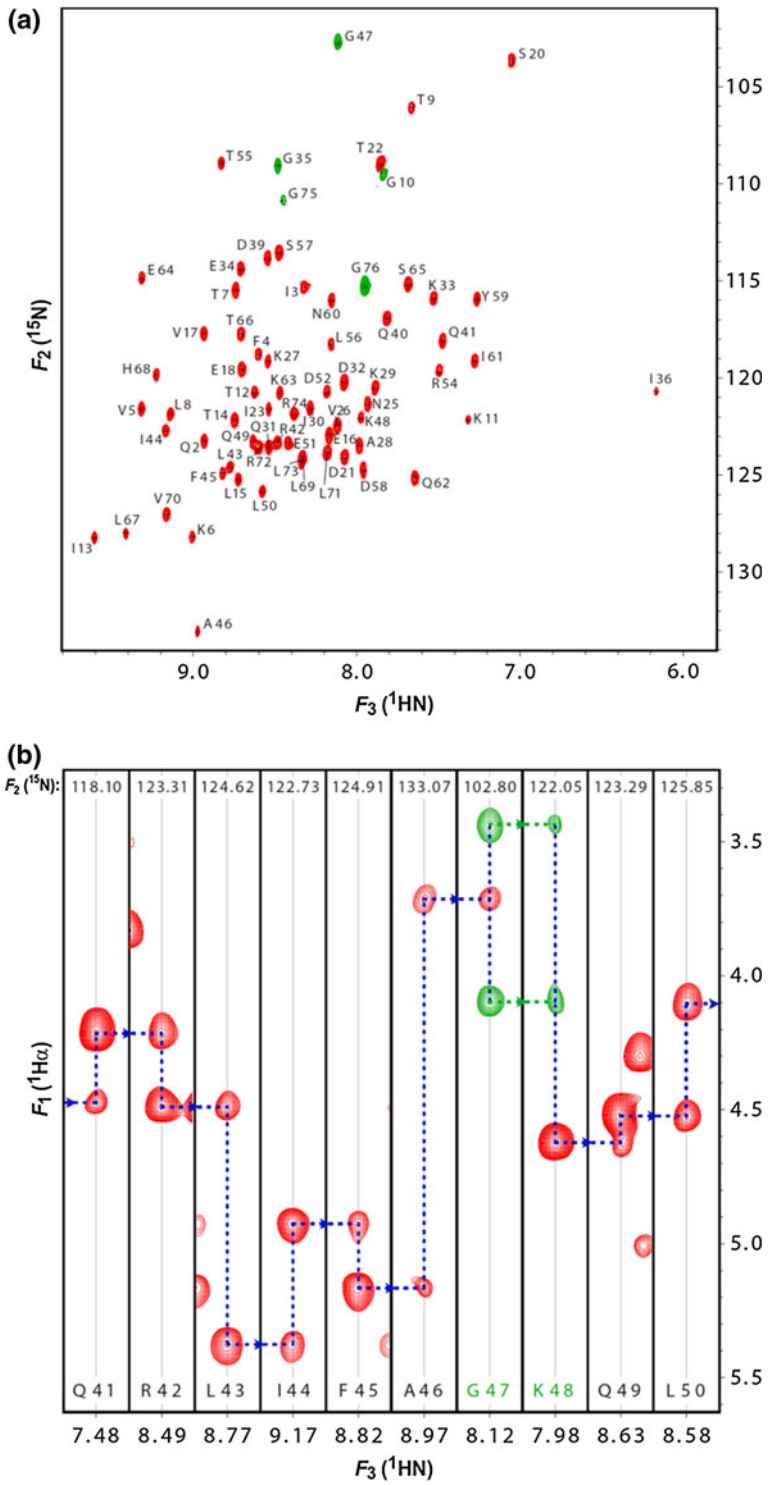

Fig. 5 **a** $F_2(^{15}N)$–$F_3(^{1}HN)$ projection plane of the 3D-HA(CA)NH data set recorded on human ubiquitin. It provides identification of backbone ^{1}HN–^{15}N correlation peaks like in ^{15}N–HSQC spectrum. **b** Illustrative stretches of sequential connection through $F_1(^{1}H\alpha)$–$F_3(^{1}HN_i)$ strips centered at $F_2(^{15}N_i)$ of the 3D-HA(CA)NH data set for residues Gln41–Leu50. The *red* and *green* contours indicate positive and negative peaks, respectively. The strips provide identification of self (i) and sequential ($i - 1$) α-proton chemical shifts. The labels (*bottom*) and numbers (*top*) present in each panel identify the residue and the respective $F_2(^{15}N)$ chemical shifts, respectively. A horizontal line connects a self peak in one plane to a sequential peak in the adjacent plane on the right. The negative peaks (shown in *green*) in both spectra are of glycine check points

low compared to the individual acquisitions (dashed lines in Fig. 4), but, one should also note that the experimental time for separate data collection is at least twice of what would be required in the present experiment. Moreover, in our scheme, both the 3D-spectra carry Gly specific checkpoint information (Ala and Ser/Thr specific information can also be easily incorporated by simple manipulations) (Chugh and Hosur 2008), which is mainly arising because of the time period where polarization sharing is happening and this is a major advantage for sequence specific resonance assignments. This offsets the slight loss of sensitivity in the present scheme. Moreover, the experiment presented in this paper demonstrates a new paradigm for parallel acquisition of multidimensional NMR spectra. Using dual

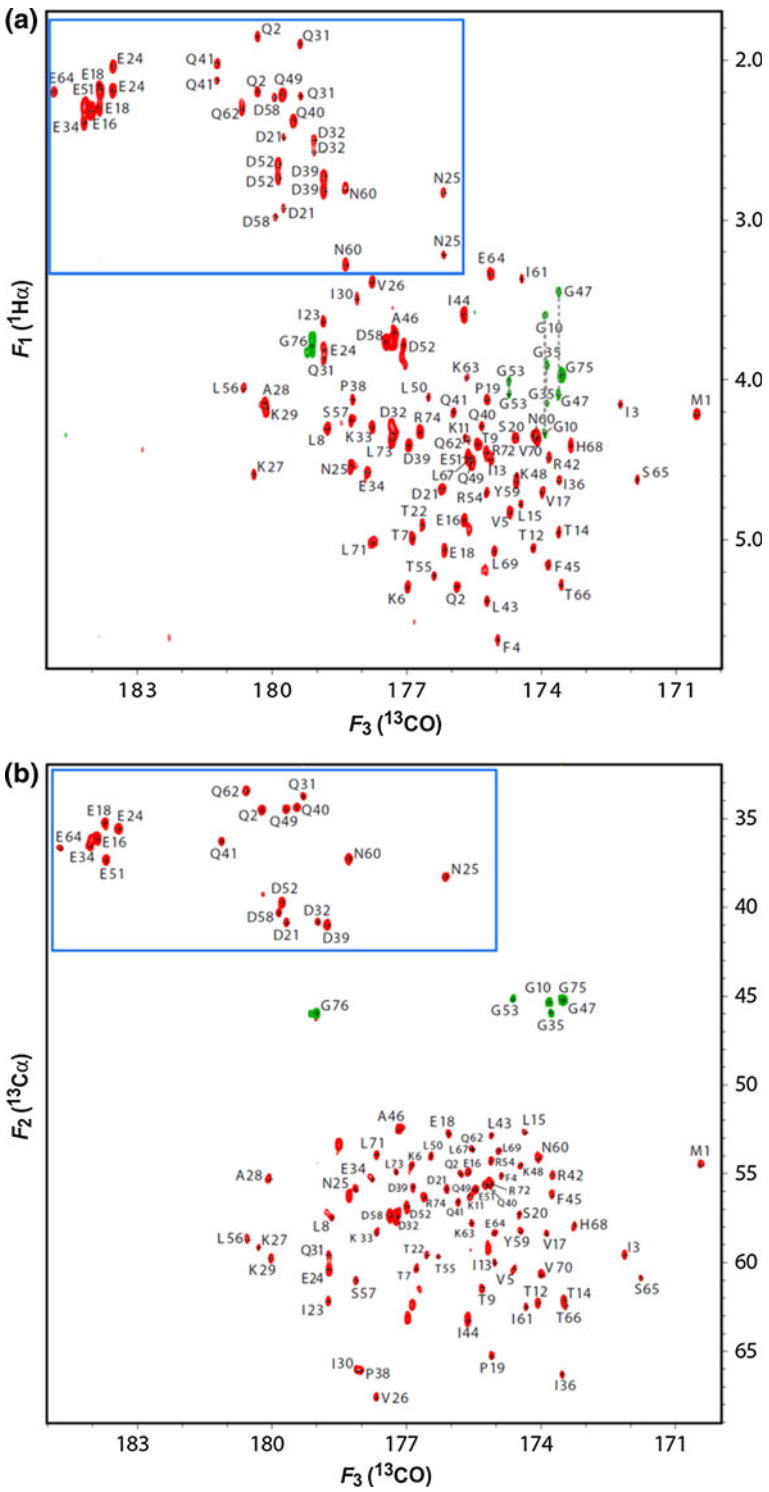

Fig. 6 **a** $F_1(^1\text{H}\alpha)$–$F_3(^{13}\text{CO})$ and **b** $F_2(^{13}\text{C}\alpha)$–$F_3(^{13}\text{CO})$ projection planes of 3D-HACACO data set recorded on human ubiquitin. The *red* and *green* contours indicate positive and negative peaks, respectively. Peaks shown in *green* are coming from glycine check points. Additionally, peaks shown in *blue boxes* originate from side chains of residues having H–C–CO network, i.e., ^{1}Hβ, ^{13}Cβ and ^{13}COγ of Asp(D) and Asn(N), and ^{1}Hγ, ^{13}Cγ and ^{13}COδ of Glu(E) and Gln(Q)

receivers which would enable different magnetization transfer pathways, a great variety of experiments with specific advantages can be designed.

The 3D-HA(CA)NH‖3D-HACACO pulse sequence (Fig. 2) was tested and demonstrated with 1.2 mM uniformly ^{15}N/^{13}C labeled human ubiquitin dissolved in acetate buffer pH 5.0 in 90 % H_2O and 10 % D_2O. All NMR experiments were performed at 25 °C on a Bruker Avance III spectrometer equipped with a RT TBI-probe, operating at ^{1}H frequency of 700 MHz For the 3D-HA(CA)NH‖3D-HACACO experiment the spectral width(offset) in ppm along the ^{1}Hα, ^{15}N, ^{1}HN, ^{13}Cα and ^{13}CO dimensions, respectively, were 7.0 (4.7), 34.0 (117.5), 11.0 (4.7), 40.0 (40.0) and 24 (172.0). These two data sets were recorded

with 1,024 complex points along the direct dimensions and 64 complex points along both the indirect dimensions. For each increment, 16 scans were accumulated. The recycling delay was set to 1.0 s. The two data sets were recorded in parallel as described above in a total measurement time of approximately 23 h 10 min. All the spectra were processed using Topspin (BRUKER, http://www.bruker.com/) and analyzed using CARA (Kellar 2004).

The proton-detected 3D-HA(CA)NH spectrum and the carbon-detected 3D-HACACO spectrum are shown in Figs. 5 and 6, respectively. The 3D-HA(CA)NH spectrum provides ^{1}Hα, ^{15}N and ^{1}HN correlations along the F_1, F_2 and F_3 dimensions, respectively. F_2–F_3 projection plane (Fig. 5a) of the spectrum displays ^{1}HN and ^{15}N correlations of all amino acids except proline (like ^{15}N-HSQC spectrum). In the F_1–F_3 planes of the 3D-HA(CA)NH spectrum, sequential '$i - 1 \rightarrow i$' correlations are observed along the ^{1}Hα dimension. An illustrative stretch of sequential walk from these planes through the spectrum of human ubiquitin is shown in Fig. 5b. A self (i) peak in one plane connects to the sequential ($i - 1$) correlation peak in the adjacent plane on the right. From these figures, it is clear that glycines make an important difference in the peak patterns. This arises due to the absence of Cα–Cβ coupling evolution during the '$2\tau_{CN}$' period (Chugh and Hosur 2008). Note that the G47–Q48 panels in Fig. 5b act as start/check points in the sequential walk, and the absence of sequential peaks will break the sequential walk, which is mostly due to presence of proline in the ($i + 1$) position.

The 3D-HACACO spectrum provides ^{1}Hα, ^{13}Cα and ^{13}CO correlations along the F_1, F_2 and F_3 dimensions, respectively. The F_1–F_3 and F_2–F_3 projection planes of the 3D-HACACO spectrum displaying ^{1}Hα–^{13}CO and ^{13}Cα–^{13}CO correlations of all amino acids including prolines are shown in Fig. 6a, b, respectively. The 3D-HACACO data set also provides information on side chains of residues having H–C–CO network (i.e., ^{1}Hβ, ^{13}Cβ and ^{13}COγ of Asp and Asn, and ^{1}Hγ, ^{13}Cγ and ^{13}COδ of Glu and Gln), as shown in blue boxes in Fig. 6. We may point out that the two α-protons of most of the glycines present in the polypeptide sequence show different chemical shifts (see Figs. 5b, 6a), which reflects their non-equivalence. Similarly, the two β-protons of Asp and Asn side chains and the two γ-protons of Glu and Gln side chains also show different chemical shifts (Fig. 6a).

In summary, we have described here a dual-receiver based parallel-acquisition pulse sequence which results in two 3D-spectra yielding five different chemical shifts (^{1}HN, ^{15}N, ^{13}CO, ^{13}Cα and ^{1}Hα) and also sequential walk through one of them (Hα). The two 3D-spectra acquired this way, as against independent acquisitions, have special spectra features (Gly specific peak patterns) which offer a significant advantage in sequential resonance assignments. With the prospect of further development in the ^{13}C detection methods and fast acquisition methods we expect such experiments to emerge more and more in the near future.

Acknowledgments We thank Government of India for providing financial support to the National Facility for High Field NMR at Tata Institute of Fundamental Research, India.

References

Andersson P, Weigelt J, Otting G (1998) Spin-state selection filters for the measurement of heteronuclear one-bond coupling constants. J Biomol NMR 12(3):435–441. doi:10.1023/A:1008239027287

Atreya HS, Szyperski T (2005) Rapid NMR data collection. Method enzymol 394:78–108. doi:10.1016/S0076-6879(05)94004-4

Borkar A, Kumar D, Hosur RV (2011) AUTOBA: automation of backbone assignment from HN(C)N suite of experiments. J Biomol NMR 50(3):285–297. doi:10.1007/s10858-011-9518-0

Chakraborty S, Paul S, Hosur RV (2012) Simultaneous acquisition of C-13(alpha)-N-15 and H-1-N-15-N-15 sequential correlations in proteins: application of dual receivers in 3D HNN. J Biomol NMR 52(1):5–10. doi:10.1007/s10858-011-9596-z

Chugh J, Hosur RV (2008) Spectroscopic labeling of A, S/T in the H-1-N-15 HSQC spectrum of uniformly (N-15-C-13) labeled proteins. J Magn Reson 194(2):289–294. doi:10.1016/j.jmr.2008.07.022

Emsley L, Bodenhausen G (1990) Gaussian pulse cascades—new analytical functions for rectangular selective inversion and in-phase excitation in NMR. Chem Phys Lett 165(6):469–476. doi:10.1016/0009-2614(90)87025-M

Frydman L, Scherf T, Lupulescu A (2002) The acquisition of multidimensional NMR spectra within a single scan. Proc Natl Acad Sci USA 99(25):15858–15862. doi:10.1073/pnas.252644399

Grzesiek S, Bax A (1993) Amino-acid type determination in the sequential assignment procedure of uniformly C-13/N-15-enriched proteins. J Biomol NMR 3(2):185–204

Hiller S, Wasmer C, Wider G, Wüthrich K (2007) Sequence-specific resonance assignment of soluble nonglobular proteins by 7D APSY-NMR spectroscopy. J Am Chem Soc 129(35):10823–10828. doi:10.1021/ja072564+

Kanelis V, Forman-Kay JD, Kay LE (2001) Multidimensional NMR methods for protein structure determination. IUBMB Life 52(6):291–302. doi:10.1080/152165401317291147

Kellar R (2004) Optimizing the process of nuclear magnetic resonance spectrum analysis and computer aided resonance assignment. Swiss Federal Institute of Technology, Zurich

Kupce E (2011) NMR with multiple receivers. Top Curr Chem. doi:10.1007/128_2011_226

Kupce E, Freeman R (2008) Molecular structure from a single NMR experiment. J Am Chem Soc 130(32):10788–10792. doi:10.1021/ja8036492

Kupce E, Freeman R (2011) Parallel receivers and sparse sampling in multidimensional NMR. J Magn Reson 213(1):1–13. doi:10.1016/j.jmr.2011.08.027

Kupce E, Kay LE (2012) Parallel acquisition of multi-dimensional spectra in protein NMR. J Biomol NMR 54(1):1–7. doi:10.1007/s10858-012-9646-1

Kupce E, Freeman R, John BK (2006) Parallel acquisition of two-dimensional NMR spectra of several nuclear species. J Am Chem Soc 128(30):9606–9607. doi:10.1021/Ja0634876

Kupce E, Kay LE, Freeman R (2010) Detecting the "afterglow" of 13C NMR in proteins using multiple receivers. J Am Chem Soc 132(51):18008–18011. doi:10.1021/ja1080025

Lescop E, Brutscher B (2009) Highly automated protein backbone resonance assignment within a few hours: the (BATCH) strategy and software package. J Biomol NMR 44(1):43–57. doi:10.1007/s10858-009-9314-2

Marion D, Ikura M, Tschudin R, Bax A (1989) Rapid recording of 2D NMR-spectra without phase cycling—application to the study of hydrogen-exchange in proteins. J Magn Reson 85(2):393–399. doi:10.1016/0022-2364(89)90152-2

Marx V (2013) Targeted proteomics. Nat Meth 10(1):19–22

Morris GA, Freeman R (1979) Enhancement of nuclear magnetic-resonance signals by polarization transfer. J Am Chem Soc 101(3):760–762. doi:10.1021/Ja00497a058

Ottiger M, Delaglio F, Bax A (1998) Measurement of J and dipolar couplings from simplified two-dimensional NMR spectra. J Magn Reson 131(2):373–378. doi:10.1006/jmre.1998.1361

Permi P, Annila A (2004) Coherence transfer in proteins. Prog Nucl Mag Res Sp 44(1–2):97–137. doi:10.1016/j.pnmrs.2003.12.001

Pervushin K, Vogeli B, Eletsky A (2002) Longitudinal (1)H relaxation optimization in TROSY NMR spectroscopy. J Am Chem Soc 124(43):12898–12902

Piotto M, Saudek V, Sklenar V (1992) Gradient-tailored excitation for single-quantum NMR-spectroscopy of aqueous-solutions. J Biomol NMR 2(6):661–665. doi:10.1007/Bf02192855

Reddy JG, Hosur RV (2012) Reduced dimensionality (4,3)D-HN(C)NH for rapid assignment of 1HN–15 N HSQC peaks in proteins: an analytical tool for protein folding, proteomics, and drug discovery programs. Anal Chem 84(23):10404–10410. doi:10.1021/ac302656k

Schanda P, Van Melckebeke H, Brutscher B (2006) Speeding up three-dimensional protein NMR experiments to a few minutes. J Am Chem Soc 128(28):9042–9043. doi:10.1021/ja062025p

Shaka AJ, Keeler J, Freeman R (1983a) Evaluation of a new broad-band decoupling sequence—waltz-16. J Magn Reson 53(2):313–340. doi:10.1016/0022-2364(83)90035-5

Shaka AJ, Keeler J, Frenkiel T, Freeman R (1983b) An improved sequence for broad-band decoupling—waltz-16. J Magn Reson 52(2):335–338. doi:10.1016/0022-2364(83)90207-X

Shaka AJ, Barker PB, Freeman R (1985) Computer-optimized decoupling scheme for wideband applications and low-level operation. J Magn Reson 64(3):547–552. doi:10.1016/0022-2364(85)90122-2

Szyperski T, Wider G, Bushweller J, Wüthrich K (1993) 3D 13C–15 N-heteronuclear two-spin coherence spectroscopy for polypeptide backbone assignments in 13C–15 N-double-labeled proteins. J Biomol NMR 3(1):127–132. doi:10.1007/bf00242481

Wagner G (1997) An account of NMR in structural biology. Nat Struct Biol 4:841–844

Yang DW, Venters RA, Mueller GA, Choy WY, Kay LE (1999) TROSY-based HNCO pulse sequences for the measurement of (HN)-H-1-N-15, N-15-(CO)-C-13, (HN)-H-1-(CO)-C-13, (CO)-C-13-C-13(alpha) and (HN)-H-1-C-13(alpha) dipolar couplings in N-15, C-13, H-2-labeled proteins. J Biomol NMR 14(4):333–343. doi:10.1023/A:1008314803561